scientific reports

Check for updates

OPEN

Acid Red 88 biodegradation by Cu nanoparticles stabilized on *Marinospirillum alkaliphilum* strain N

Samira Eshghi & Fereshteh Jookar Kashi✉

In recent years, Cu nanoparticles (CuNPs) have emerged as a widely used and cost-effective tool, especially in analytical fields. This study investigates the biological properties of CuNPs synthesized by strain Cu1 and their efficiency in degrading Acid Red 88 dye. Additionally, it evaluates the potential of a novel combination of *Marinospirillum alkaliphilum* strain N and CuNPs for AR88 biodegradation. Strain Cu1, a copper-resistant strain from the Sungun copper mine, was used for biosynthesizing CuNPs, with 16S rDNA sequence analysis showing a 99.10% similarity to *Micrococcus lylae*. Characterization via UV–Vis, FTIR, XRD, and SEM–EDX confirmed that the CuNPs were spherical-shaped and ranged in size from 20 to 100 nm. These nanoparticles demonstrated antimicrobial effects against various bacteria. The cell free extract/CuNPs and biomass/CuNPs of the degrading *Marinospirillum alkaliphilum* strain N achieved 100% degradation of Acid Red 88 within 11 h. In contrast, cell free extract and the biomass of strain N alone required 24 h to achieve the same result. FTIR and GC–MS analyses verified the degradation of AR88 dye. Toxicity assessments using *Artemia salina* and radish seeds revealed that Acid Red 88 dye was toxic. In contrast, metabolite biodegradation and CuNPs exhibited low toxicity, no mortality of *A. salina*, and no inhibiting seed germination.

Keywords CuNPs, Dye degradation, Immobilization, Antimicrobial assay, Toxicity

Abbreviations

AR88	Acid Red 88
CFE	Cell free extract
CuNPs	Cu nanoparticles
GC-MS	Gas chromatograph mass spectrometer
BST	Brine shrimp lethality assay
M-BD	Metabolite biodegradation
IN-M	Intracellular metabolites
EM-EDX	Scanning electron microscope-energy dispersive X-ray espectroscopy
FTIR	Spectrometer Infrared Fourier Transform
RSG	Relative seed germination
RRG	Relative root growth
GI	Germination index
NA	Nutrient agar
NB	Nutrient broth

Dyes from industries like textile, automotive, or cosmetics are polluting our sewage. New inexpensive methods to remove high-yield dye impurities are being developed as a solution[1]. The textile industry has not used all physicochemical decolorization techniques for the last two decades. Their non-implementation was mainly due to many dyes' high cost, low efficiency, and impracticability[2]. The ability of microorganisms to perform decolorization has received much attention. Decolorization and microbial degradation of dye are considered cost-effective methods to remove these contaminants from the environment[3]. Also, microorganisms do not quickly degrade textile dyes. Research has shown that microorganisms can destroy various dyes. However, this method is not desirable due to the production of aromatic amines. Amine components may be toxic and carcinogenic[4].

Department of Cell and Molecular Biology, Faculty of Chemistry, University of Kashan, Ootb-E Ravandi Blvd, Kashan, Isfahan, Iran. ✉email: Jookar@kashanu.ac.ir

Azo compounds, synthetic inorganic chemical compounds, comprise 70% of the dyes used today. According to studies, 10–15% of the dye used in textile processing is lost and released as effluent. Various microbial species such as bacteria, fungi, yeasts, algae, and actinomycetes can degrade azo dyes. In the meantime, bioremediation by bacteria is much faster and leads to better decolorization efficiency[5–14]. Microorganisms can survive in harsh conditions and contaminated environments, allowing them to produce novel enzymes and metabolites that can help tackle environmental issues. Bioremediation utilizes these microorganisms as a viable alternative to traditional physicochemical methods. They can effectively break down polyaromatic hydrocarbons, transform heavy metals into less harmful states, degrade pesticides, and reduce or eliminate azo dyes. The processes for removing dyes involve both adsorption and enzymatic degradation. While adsorption operates through ion exchange, it does not convert azo dyes into non-toxic forms. In contrast, microbial enzymatic degradation can fully break down these dyes[15]. Copper has been known and utilized as an antimicrobial agent since ancient times. Today, copper-based nanoparticles with antimicrobial properties are extensively used across various sectors of daily life. Due to their unique properties, these nanoparticles are particularly effective in combating harmful microorganisms[16].

Copper nanoparticles are particles of 1 to 100 nm[17]. Biological or chemical processes were applied in the formation of copper nanoparticles. Copper nanoparticles were formed via biological or chemistry methods, like other nanoparticles. Nanoparticles are used as dyes and biomedical agents due to their unique properties[18]. Green nanotechnology provides eco-friendly solutions, reducing reliance on toxic chemicals and finding applications in environmental remediation and sustainable energy development. Bioreduction is a sustainable alternative to chemical reduction, avoiding harmful reducing agents and instead using environmentally friendly substances. This method controls the size and shape of nanoparticles by adjusting the concentration of biological extracts and adding natural reducing agents[19]. Copper nanoparticles have unique properties like catalytic, antifungal, and antibacterial activity. They have a large catalytic surface and small and high porosity, which makes them more efficient and faster in synthesizing organic and metallic metals. For instance, copper nanoparticles achieved 88% conversion to biphenyl in the iodobenzene compaction reaction, while commercial copper only managed a 43% conversion rate[20]. Small copper nanoparticles have a potent effect against bacteria and fungi. Their interaction with microbial membranes and release of metal ions in solutions causes significant antimicrobial activity, making them a promising solution for infectious diseases[21]. Nanoparticles oxidizing in solutions release cupric ions that can form toxic hydroxyl free radicals near the lipid membrane. These radicals break down lipids through oxidation, ultimately destroying the membrane. As a result, intracellular material leaves the cells through damaged membranes. Free radicals damage cells, hindering their ability to maintain basic biochemical processes. Eventually, intracellular changes occur, leading to cell death[22]. Copper oxide nanoparticles are used in industrial production, and releasing these nanoparticles into the environment causes toxicity to aquatic organisms. Copper oxide nanoparticles are used in skincare, oils, polymers, metal coatings, plastics, and inks. Research has shown that copper sulfate and copper oxide nanoparticles can induce genetic toxicity of cells and damage cellular DNA[23]. This study isolated copper-producing bacteria from the Songun mine, producing copper nanoparticles from strain Cu1. The antimicrobial properties and toxicity of the nanoparticles were studied. The study focused on examining the toxicity and antimicrobial properties of nanoparticles.

Materials and methods

This research used materials from Merck, Germany, and AR88 dye synthesized by Alvan Sabet in Iran. Bacterial strain N was acquired from the microorganism collection at Kashan University, isolated from Kashan textile effluent, and identified as *Marinospirillum alkaliphilum* at 97.24% similarity.

Isolation of bacteria

Bacterial strains from Sungun copper mine slime were cultured on $CuCl_2$-supplemented nutrient agar at 30 °C for 24 h. Strain Cu_1-copper resistance was selected for further study. Experiments were conducted on strain Cu_1 using standard assays for phenotypic designation, including oxidase, catalase, cell morphology, and gram-staining. Strain Cu1 chromosomal DNA was extracted using the Marmur method[24]. 16S rDNA genes were amplified with 27 F and 1492 R primers[25,26], followed by sequence analysis using ChromasPro software and the BLASTn sequence adjustment assay on the EzBioCloud site. Coordination was done using Bioedit software. MEGA X software was used for phylogenetic analysis. A thousand replicates of bootstrap values constructed the evolutionary history. Tajima-Ney assay studied base switches and evolution distances[27].

Bacterial synthesis of CuNPs

Bacterial strain Cu1 was cultured in 50 ml of nutrient broth and incubated in a shaker at 30 °C with a speed of 120 rpm for 24 h. After incubation, the bacterial suspension was centrifuged at 7000 rpm for 15 min at 4 °C to separate CFE from IN-M. The collected supernatant was then utilized for synthesizing copper nanoparticles[28]. To achieve this, 50 ml of 2 mM $CuCl_2$ solution was mixed with 1 ml of CFE. The biosynthesis of CuNPs was studied using UV–Vis (300–800 nm) after a color change due to exposure to light. After 6 h, NPs separated from CuCl2 solutions centrifuged (12,000 rpm, 20 min) and then dried at 60 °C in an oven for 24 h. Mix the dried NPs powder with 2 ml of distilled water and 10 ml of 96% ethanol, and sonicate the mixture 20 times for 2 min in a container for perfect consistency. CuNPs were thoroughly investigated using FTIR, XRD, and SEM–EDX after sonication, drying for 24 h at 60 °C and placing in a kiln for 5 h at 450 °C. Average NPs size was calculated using Debye–Scherrer Eq. (1)[29]:

$$\mathrm{D} = 0.94\lambda / \beta \cos \theta, \tag{1}$$

where D is the crystal size, β is full width at half maximum (FWHM), λ is the X-ray wavelength, and Θ shows the diffraction angle.

Antimicrobial assay

CuNPs were tested as antimicrobial agents on standard strains using a diffusion assay. Strains tested: *Escherichia coli* (ATCC 10536), *Staphylococcus aureus* (ATCC29737), *Shigella dysenteriae* (PTCC1188), *Salmonella paratyphi-A serotype* (ATCC 5702), and *Candida albicans* (ATCC 10231). CuNPs were used to inhibit bacterial growth on nutrient agar. The plates were inoculated with 0.5 McFarland bacterial suspension, and 20 µl of CuNPs (30 mg/ml) was placed into wells and incubated for 24 h at 30 °C. The study measured the inhibition zone diameter and examined the antimicrobial activity of AR88 and M-BD through diffusion assay on standard strains. 10 µl of AR88 and M-BD (20 mg/ml) were incubated in wells at 30 °C for 24 h; then, the inhibition zone diameter was recorded.

Toxicity assay

The toxicity of AR88, BD-P, and CuNPs was assessed using lethality tests on saltwater shrimp larvae and *Raphanus sativus* L. seeds. For the shrimp hatching procedure, 0.1 g of shrimp eggs were exposed to light in a saltwater aquarium for 48 h, with continuous aeration maintained at 30 °C. The experimental setup involved glass tubes filled with saltwater at a pH of 9.0. Ten shrimp larvae were exposed to different concentrations (25–2500 µg/ml) of CuNPs and AR88 dye M-BD. After 24 h, the number of live and dead larvae was recorded in a 30 °C water bath under light after soaking the larvae in brine. The experiment was repeated three times to ensure accuracy and reproducibility. Ten live larvae were used for control, along with 5 ml of saline water in each sample. The mortality rate was calculated using the formula (2)[30]:

$$\text{Percentage of dead larvae after 24 h} = [(\text{m} - \text{M})/\text{S}] \times 100, \tag{2}$$

m: The average number of dead larvae in the samples, M: Mean number of dead control larvae, S: The average number of live control larvae.

Biotoxicity of AR88, M-BD, and CuNPs was assessed on *Rhaphanus sativus* L. seeds using sterilized filter paper placed in plates through an autoclave from Abzar Teb Mahan, Iran. The seeds were soaked in 70% alcohol for 1 min, UV-exposed for 90 min in Laminar Flow II (120RS, Jal Tab, Iran), rinsed in distilled water (10 min), and bleached (20%) for 5–6 s. Samples (5 ml) were added to plates with seeds for toxicity assessment. Distilled water was used as a control. Seeds were exposed to sunlight for eight days. This experiment analyzed seed growth by examining the number of leaves, roots, and stems and analyzed using formula (3) to examine RSG, RRG, and GI[27]:

$$\text{RSG} = \frac{Number\ of\ germinated\ seeds\ in\ aqueous\ extract}{Number\ of\ germinated\ seeds\ in\ deionized\ water\ (control)} \times 100\%, \tag{3}$$

$$\text{RRG} = \frac{Radicle\ length\ of\ germinated\ seeds\ in\ aqueous\ extracts}{Radicle\ length\ of\ germinated\ seeds\ in\ deionized\ water\ (control)} \times 100\%,$$

$$\text{GI} = \text{RSG} \times \text{RRG} \times 100\%.$$

Bioremediation of AR88 using CFE and CuNPs CFE

A mix of 10% peptone, 0.5% yeast extract, and 1% glucose at pH 7 was used to grow Strain N in an Erlenmeyer flask. The flask was incubated at 37 °C and 150 rpm for 24 h. After that, it was centrifuged at 6000 rpm for 15 min at 4 °C. After 24 h, 100 mg/l of AR88 was added to the CFE and incubated at 30 °C. Moreover, bioremediation of AR88 was evaluated using CFE /CuNPs.Steps were repeated, and CuNPs (30 mg/ml) were added to CFE. Results were analyzed via UV–Vis. The percentage of BD was determined by Formula (4)[28]:

$$\text{Biodegradation efficiency}\ (\%) = \frac{Initial\ absorbance - Final\ absorbance}{Initial\ absorbance} \times 100 \tag{4}$$

Bioremediation potential CuNPs/strain N

Strain N biomass was separated via centrifuge at 5000 rpm and mixed with CuNPs powder (30 mg/ml) in PBS buffer. The solution was incubated at 30 °C with 100 mg/l AR88 and 50 mg/l glucose for 13 h to bioremediate AR88 dye. The results were evaluated using UV–Vis, and % BD was determined by Formula (4). Fixation of CuNPs on strain N was investigated using SEM–EDX analysis.

Decolorization metabolites assay

Strain N was used to treat the AR88 dye solution, and decolorization products were extracted through centrifugation at 1000 rpm, 8 min, and 4 °C. The metabolites were effectively dissolved by vigorously shaking 10 ml of the supernatant with an equal volume of ethyl acetate. To identify intermediates, the organic phase was separated, evaporated, dissolved in methanol, dried with Na_2SO_4, and analyzed by FTIR and GC–MS[31].

Statistical analysis

In this study, all tests were conducted in triplicate, and the results were reported as mean ± standard deviation. Data analysis was performed using GraphPad Prism version 10.4.1, and the significance of the differences was evaluated using ANOVA analysis followed by the Tukey post-hoc test.

Results and discussion

Identification of CuNPs-synthesizing bacterial strain Cu1

A copper-resistant bacterial isolate was chosen among isolates screened from samples collected from the Songun copper mine to synthesize CuNPs. Figure 1 shows the use of the GenBank database to analyze the relationship between strain Cu1 and nucleotide sequences of other strains. Bacterial strain Cu1 was related to the *Micrococcus* genus and had a 99.10% similarity with *Micrococcus lylae* NBRC 15355 (T). Strain Cu1 is a candidate for new species, with its 16S rDNA gene sequence linked to the gene bank (https://www.ncbi.nlm.nih.gov), access number OR421360. 16S rDNA gene sequence of strain Cu_1 is linked to the gene bank https://www.ncbi.nlm.nih.gov, access number OR421360, indicating it is a candidate for new species.

Synthesis and characterization of Cu_2O-NPs

A comprehensive physicochemical analysis was conducted to characterize copper nanoparticles (CuNPs) biosynthesized using bacterial culture, as illustrated in Fig. 2.

UV–Vis spectroscopy

The UV–visible absorption spectra (Fig. 2A) revealed two distinct but complementary phenomena. First, the characteristic surface plasmon resonance (SPR) band observed between 580 and 600 nm confirmed the successful biosynthesis of CuNPs, with peak intensity increasing over time and reaching a maximum at 120 h. A slight red-shift in the SPR peak position suggests particle growth or aggregation, consistent with previous studies[32–34].

In parallel, the absorption spectra demonstrated a gradual decrease in the dye peak around 510–520 nm during the decolorization of AR88 over 24, 48, 72, and 120 h, indicating progressive biodegradation by bacterial strain N. Gaussian fitting curves further confirmed the temporal decline in chromophore intensity, which was visually supported by the fading color of the solution (Fig. 2A). These results suggest the simultaneous synthesis of CuNPs and degradation of dye molecules, highlighting the multifunctional capability of the strain.

FTIR analysis

Fourier-transform infrared (FTIR) spectroscopy (Fig. 2B) was performed to elucidate the functional groups involved in dye degradation and nanoparticle biosynthesis. The untreated bacterial supernatant (spectrum b) exhibited typical peaks at 3434 cm^{-1} (O–H stretching), 2906 cm^{-1} (C–H stretching), 1657 cm^{-1} (amide I, C=O stretching), and 1404 cm^{-1} (amide II, C–N stretching), indicative of proteins, carbohydrates, and other cellular metabolites.

After CuNP formation (spectrum a), notable reductions in the intensity of amide bands and the emergence of a new peak at 616 cm^{-1}—assigned to Cu–O bonding—were observed, signifying the involvement of biomolecules in nanoparticle stabilization. Additionally, FTIR analysis of decolorized dye samples revealed the disappearance or shifting of azo and aromatic group peaks, supporting the chemical breakdown of AR88 by bacterial action. These spectral changes collectively underscore the role of microbial metabolites in both the biotransformation of pollutants and nanoparticle formation.

XRD analysis

X-ray diffraction patterns (Fig. 2C) confirmed the crystalline nature of the biosynthesized CuNPs. Diffraction peaks at 2θ values of approximately 43.4°, 50.5°, and 74.2° correspond to the (111), (200), and (220) planes of face-centered cubic (FCC) copper, aligning with standard JCPDS card No. 04-0836. The absence of peaks for Cu_2O or CuO phases suggests the predominant presence of metallic copper. Peak broadening is indicative of nanoscale crystallinity. The average crystallite size was estimated at 27.88 nm using the Debye–Scherrer equation. In a related study, Ashrafi et al. characterized Ag/CuO nanoparticles in epoxy composites and confirmed their presence through multiple XRD peaks[35].

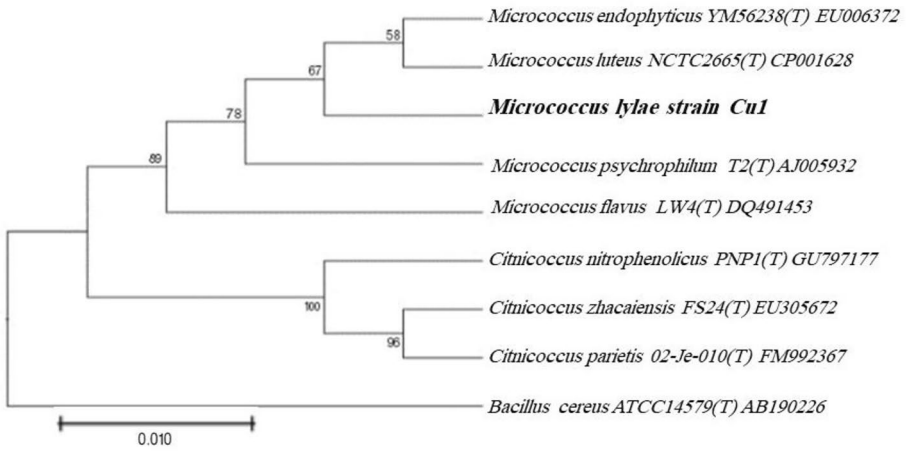

Fig. 1. The phylogenetic tree shows the relation of strain Cu1 with similar strains in GenBank.

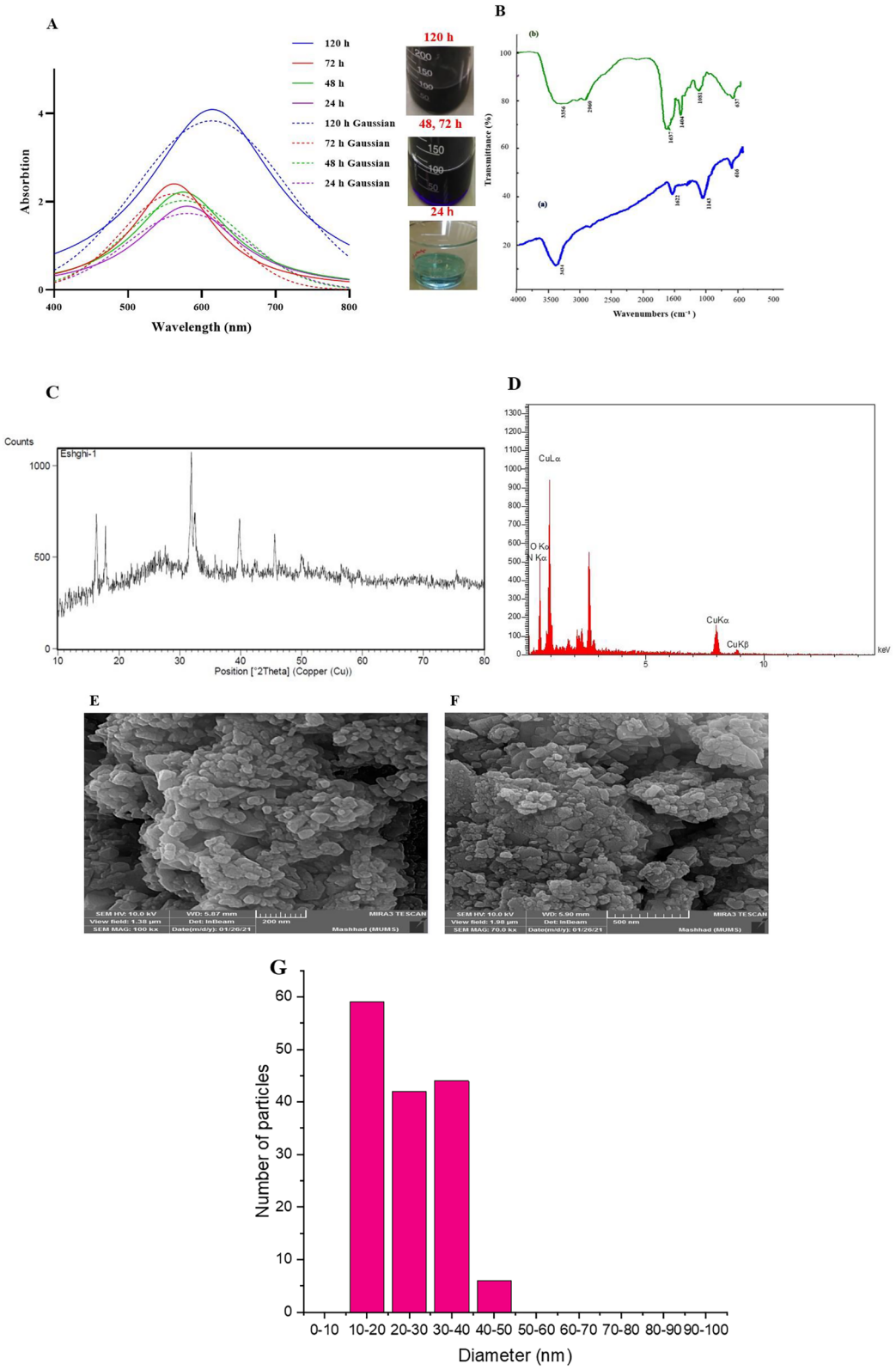

Fig. 2. (**A**) UV–Vis absorption spectra showing the decolorization of AR88 dye over time (24, 48, 72, and 120 h) using the bacterial treatment. The corresponding Gaussian fitting curves demonstrate the progressive decrease in absorption, particularly around 510–520 nm, indicating effective dye degradation. Inset images show the visual color change of the dye solution at different time points. (**B**) FTIR spectra of (a) untreated AR88 dye and (b) bacterial decolorization product after 120 h, indicating changes in functional groups due to biodegradation, including the disappearance or shifting of characteristic azo and aromatic peaks, XRD pattern of CuNPs produced using strain Cu1 (**C**), EDX spectrum (**D**), SEM images of CuNPs produced using the CFE by strain Cu_1 (**E,F**), and Biosynthesized CuNPs size distribution (**G**).

EDX analysis

Energy-dispersive X-ray spectroscopy (Fig. 2D) revealed copper as the predominant element (52.6 wt%), with substantial amounts of oxygen (33.6 wt%), carbon (7.7 wt%), and nitrogen (6.1 wt%). The oxygen signal may stem from partial surface oxidation or organic capping agents. The detection of carbon and nitrogen further supports the role of biomolecules—likely proteins and polysaccharides—in nanoparticle stabilization. Similar elemental compositions have been reported by Rani Verma et al. for CuO-NPs synthesized using *Prunus amygdalus* extract.

SEM analysis

Scanning electron microscopy (Fig. 2E,F) revealed predominantly spherical CuNPs with moderate agglomeration levels, typical of biologically synthesized nanomaterials. Such aggregation may arise from drying effects or limited dispersion forces without synthetic surfactants. The particle sizes, as measured from SEM images, were in agreement with the nanometric dimensions estimated from XRD data. Particle size analysis using Digimizer software showed a distribution ranging from 10 to 20 nm (minimum) to 30–40 nm (maximum), as depicted in Fig. 2G.

Collectively, the analytical data confirm the successful biosynthesis of stable, crystalline CuNPs with a predominantly metallic core and a surface layer composed of organic and/or oxidized components. The biomolecules in the bacterial culture facilitated the reduction of Cu^{2+} ions and acted as natural capping agents, contributing to the colloidal stability of the nanoparticles. These attributes underscore the potential applicability of biosynthesized CuNPs in biomedical, antimicrobial, and catalytic domains.

Antimicrobial assay of CuNPs

As shown in Fig. 3, Cu nanoparticles exhibit their antimicrobial properties by inhibiting the growth of standard bacteria around the wells. The investigation of the antimicrobial effects of AR88 and M-BD on standard strains indicated that AR88 had a strong inhibitory effect on bacteria. In contrast, M-BD showed no antimicrobial activity against the standard strains. These findings suggest that after the decolorization process, the toxicity of the dye to bacteria is reduced. This antimicrobial effect is attributed to the ability of copper to damage cellular functions, generate reactive oxygen species (ROS), and disrupt bacterial proteins and DNA. Copper damages microbial cells by generating ROS and disrupting metalloproteins, giving them antimicrobial properties. The innate immune system also enhances phagocytosis and increases ROS production, boosting bactericidal activity. Copper-containing nanoparticles (NPs) inhibit microorganisms through mechanisms similar to other copper-based materials. Numerous studies have shown that these NPs exhibit stronger antimicrobial properties than conventional copper materials, although the exact reason remains unclear. Due to their higher surface area and distinct crystalline structure, copper NPs can interact with various microbial cell components through unique mechanisms, enhancing their antibacterial effectiveness. Due to their higher surface area and unique crystal structure, CuNPs outperform regular copper materials by releasing more copper ions and triggering multiple antibacterial mechanisms, making them less susceptible to microbial resistance[36]. Hosseinzadeh et al.[37] studied the antibacterial effects of Cu_2O nanoparticles on *E. coli* and *S. aureus*, demonstrating their strong antimicrobial properties. In 2021, Rakhshan et al.[34] found Cu_2O nanoparticles effective against *B. subtilis*, while Nikouharf Fakher et al. confirmed the antibacterial activity of Ag/AgCl nanoparticle composites against pathogenic bacteria.

Various studies have explored the synthesis of nanoparticles with diverse antimicrobial and other beneficial properties[38]. Zinc oxide nanoparticles from *Talaromyces islandicus* inhibited multidrug-resistant bacteria without affecting seed germination[38]. Silver nanoparticles synthesized using *Cucumis sativus* and *Penicillium brasilianum* exhibited moderate antimicrobial and anticancer effects[39]. Silver nanoparticles from *Lagerstroemia speciosa* flower buds showed significant antimicrobial and anticancer potential[40]. However, silver nanoparticles from *Streptomyces* sp. NS-33 had antimicrobial activity but was toxic to plant cells, limiting their use[41]. *Proteus mirabilis* 10B biosynthesized CuO-NPs with strong antimicrobial properties and a pure crystalline structure[42]. Furthermore, Almahdy et al. developed a CuO-TiO_2 nanocomposite using *Candida* sp., which showed excellent stability and potent antimicrobial activity, reducing biofilm formation and microbial contamination by as much as 80%. Lastly, a CuFe hybrid nanocomposite synthesized from *Streptomyces cyaneofuscatus* exhibited significant antimicrobial, anticancer, and dye adsorption properties, effectively reducing pathogen growth by over 70% and removing 68% of dye[43].

Biotoxicity of CuNPs

Brine shrimp was used as an indicator to assess the toxicity of biosynthesized CuNPs on living organisms. The results showed that within 24 h, more than half of the shrimp died at a concentration of 0.5 µg/ml CuNPs (Fig. 4). To evaluate the toxicity of CuNPs, radish (*R. sativus* L.) seeds were also used. The RRG and RSG values for CuNPs were measured at 0.15% and 15%, respectively (Fig. 5A,B). Additionally, the germination index (GI) in the presence of CuNPs was 2.25% (Fig. 5C). The results also showed that the seed length in the control and CuNPs-treated samples was 3 cm and 2.9 cm, respectively (Fig. 5D). Various studies have investigated the toxicity of nanoparticles on plant seeds and living organisms. Mehrzad et al.[31] demonstrated that TiO nanoparticles exhibit high toxicity and reduce radish seed growth, which aligns with the findings of this study. These results highlight that the toxicity of nanoparticles varies depending on the type of organism and emphasize the importance of identifying their potential risks to the environment, food chains, and plant growth. Arumugam et al. also examined the biotoxicity of biosynthesized Cu_2O-NPs using Panchagavya through a brine shrimp assay and found that these nanoparticles exhibited very low toxicity[44]. In another study, copper diethyldithiocarbamate nanoparticles were synthesized using bacterial and green chemistry methods. The green-synthesized nanoparticles demonstrated superior anticancer effects, including apoptosis induction

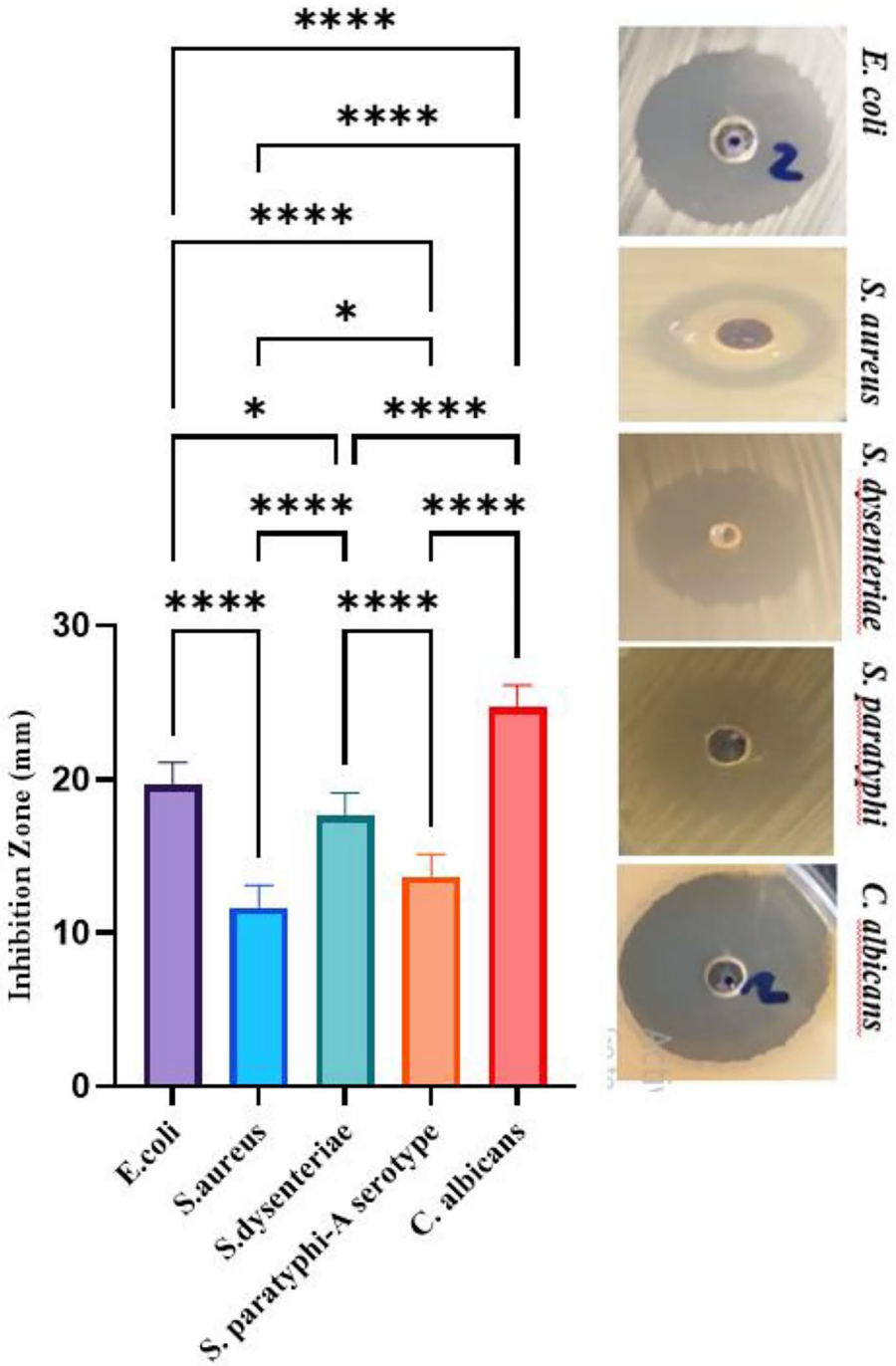

Fig. 3. The antimicrobial effects of CuNPs on standard strains. The number of stars indicates the level of significance based on Tukey's test (****P-value < 0.0001; *ns* not significant). Error bars represent the 95% confidence interval.

and inhibition of cell migration, which were attributed to their smaller size and enhanced cellular uptake[45]. In one study, a nanocomplex combining disulfiram and copper oxide nanoparticles was developed to enhance the anticancer properties of disulfiram, showing improved stability, effectiveness, and cellular absorption[46]. Another study used a microbial consortium to completely degrade methylene blue in wastewater with non-toxic byproducts, proving its effectiveness in treatment[43].

Toxicity of AR88 dye before and after biodegradation

Toxicity tests on AR88 dye and its biodegraded product (M-BD) using the BST assay revealed that AR88 exhibits high toxicity, whereas M-BD shows minimal toxicity. M-BD could not eliminate 50% of *Artemia salina* (Fig. 4). In a similar study, Mehrzad et al.[31] assessed the toxicity of Blue 41 dye before and after degradation using the

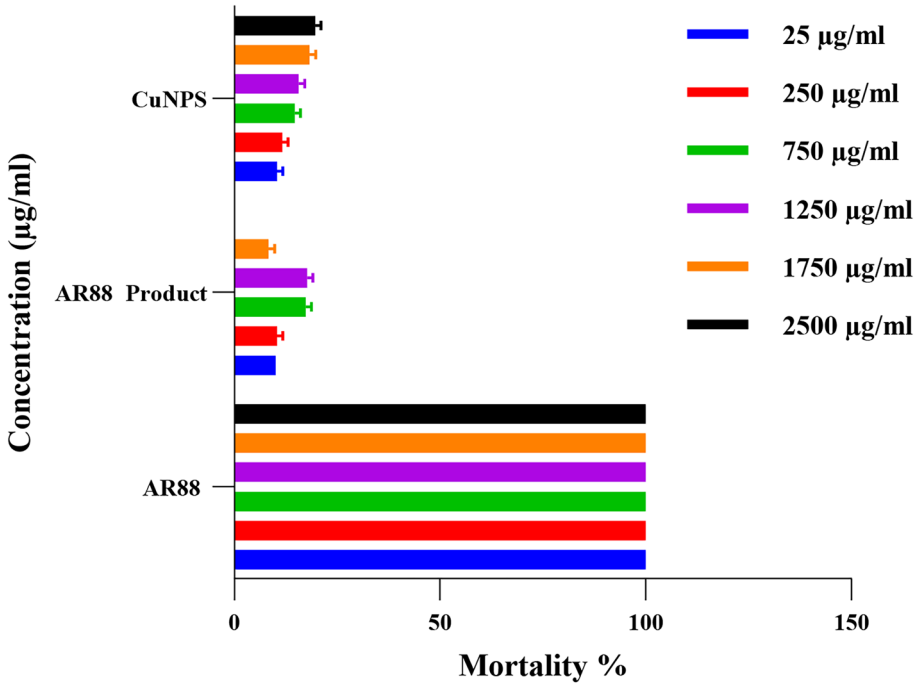

Fig. 4. Toxicity evaluations were conducted with *A. salina* after 24 h exposure to different concentrations of CuNPs, AR88, and M-BD. Error bars in the chart represent the 95% confidence intervals for the measurements.

BST assay. Their findings indicated that while Blue 41 had high toxicity, its biodegradable product (M-BD) exhibited significantly lower toxicity. To assess the toxicity of the AR88 dye and its biodegradable product (M-BD), *R. sativus* L. seeds were used. The RRG and RSG values for AR88 were calculated as 0.16% and 16%, respectively, while for BD-P, these were 0.83% and 80% (Fig. 5A,B). Additionally, the germination index (GI) for AR88 was 2.56%, whereas M-BD exhibited a GI of 66.40%. The control sample (water) showed a GI of 100% (Fig. 5C). These findings indicate that AR88 has high toxicity, significantly inhibiting seed growth, whereas the control samples exhibited proper growth. Furthermore, the measurement of radish seed length revealed that in the control, AR88, and the biodegraded AR88 product, the seed lengths were 3 cm, 0.5 cm, and 2.5 cm, respectively (Fig. 5D). Moreover, a study by Seyedi et al.[47] on the toxicity of Disperse Blue 60 dye in radish seeds demonstrated that this dye exhibits high toxicity. In contrast, its biodegradable product shows significantly lower toxicity.

Biodegradation of AR88 with CFE strain N without/with CuNPs

In the first stage, AR88 was added to the CFE of strain N. The results demonstrated that the CFE exhibited a high decolorization capability, completely degrading AR88 within 24 h. The decolorization efficiency reached 100% (Fig. 6A), and the decolorization products were illustrated using UV–Vis (Fig. 6B). In the next stage, AR88 and 30 mg/ml of CuNPs were added to the CFE. The results indicated that the CFE achieved complete AR88 decolorization within 11 h with 100% efficiency (Fig. 6C), and the decolorization profile was further analyzed using UV–visible (Fig. 6D). The metabolic degradation of AR88 by the CFE was investigated using GC–MS and FTIR analyses. The GC–MS results confirmed the complete degradation of AR88 (Fig. 8B). The degradation pathway of Acid Red 88 (Fig. 8A) revealed its breakdown into various low-molecular-weight compounds. Acid Red 88, which contains sulfonate groups and aromatic rings, was enzymatically converted into several intermediate compounds. These included (Z)-1-hydrazono-1,8a-dihydronaphthalen-2(4aH)-one, which features a naphthalene ring with a hydrazono group and specific oxygen positions, and sodium naphthalene-1-sulfonate, which consists of a naphthalene ring with a sulfonate group. Further enzymatic processing led to the formation of (Z)-6-hydrazono cyclohex-2-enone and sodium benzenesulfonate. This degradation pathway breaks down Acid Red 88 into simpler, lower-molecular-weight molecules.

FTIR spectroscopy analysis indicates that the absence of specific peaks in the 670–870 cm^{-1} range signifies the complete decomposition of aromatic structures associated with benzene rings. This process leads to the breakdown of aromatic frameworks, while functional groups attached to these rings detach due to N-induced strain. Removing the C-NH_2 peak in the 1031–1118 cm^{-1} range confirms this phenomenon. Additionally, the reduction in the peak intensity above 3000 cm^{-1}, corresponding to N–H vibration, is evident after the decolorization process. The disappearance of the peak in the 1210–1320 cm^{-1} range further indicates the elimination of the C–O bond in the final products. Moreover, the emergence of a peak in the 1620–1680 cm^{-1} region suggests the formation of C=C bonds, while the reduction of the N–O bond peak in the 1515–1560 cm^{-1} range demonstrates its presence in the initial dye spectrum but not in the final product. In the spectrum of

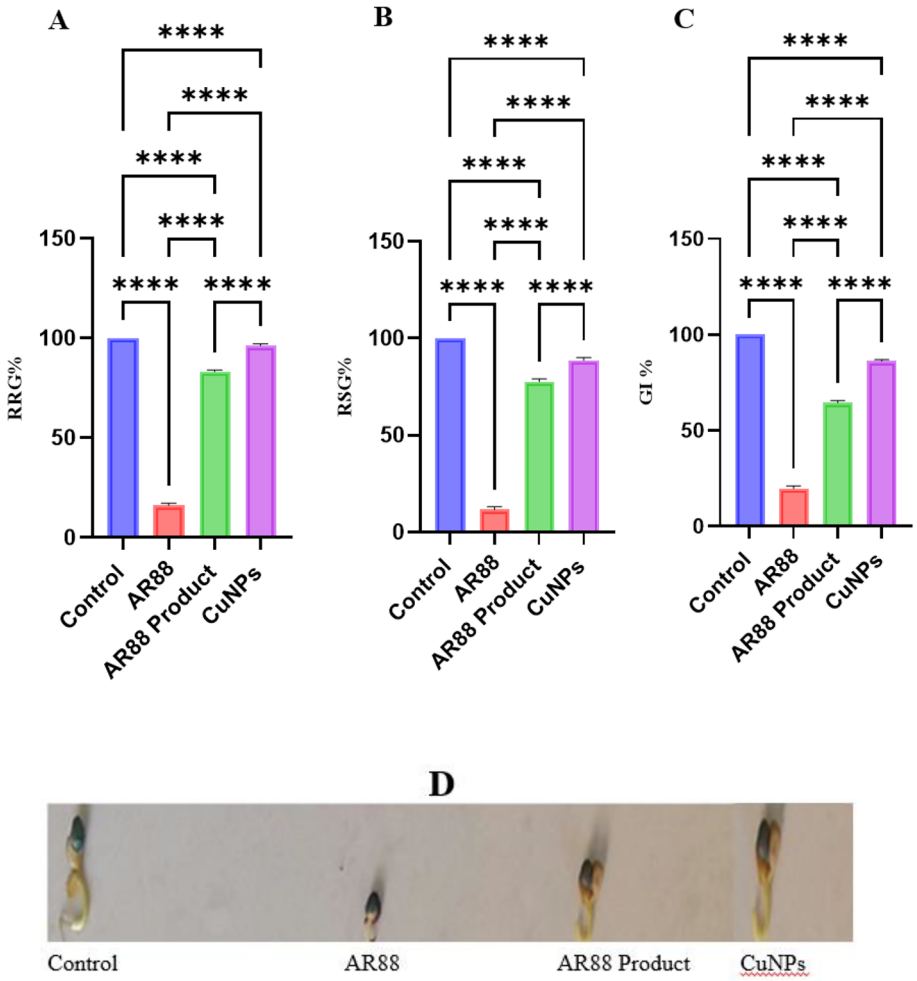

Fig. 5. Evaluation of biotoxicity using radish seeds after seven days of sun exposure (comparison of RRG (**A**), RSG (**B**), and (comparison of GI) (**C**), The sizes of radish seeds are in order from the left control H_2O (3 cm), AR88 dye (0.5 cm), AR88 product (2.5 cm), and CuNPs (2.9 cm), respectively (**D**). The number of stars indicates the level of significance based on Tukey's test (****P-value < 0.0001; *ns* not significant). Error bars in the chart represent the 95% confidence intervals for the measurements.

AR88 dye, a distinct peak in the 1578–1611 cm^{-1} range corresponds to the azo bond. The disappearance of this peak in the decolorized products suggests the complete breakdown of the azo bond. Other observed peaks are related to C–H stretching vibrations (Fig. 7). Additionally, the degradation pathway of AR88 is explicitly illustrated in Fig. 8A. Previous studies have demonstrated the effectiveness of various bacterial strains in the biodegradation of industrial dyes. Nazari et al.[48] achieved 100% decolorization of Disperse Blue 183 using *Enterococcus casseliflavus* A2, with GC–MS confirming complete dye degradation. In another study, Nazari et al.[49] reported that *Enterobacter cloacae*, immobilized in Ca/Alg beads, efficiently decolorized Reactive Blue 19, as verified by FTIR and GC–MS. Similarly, Seyedi et al.[50] found that bacterial strains from Kashan textile effluent successfully removed Reactive Red 152 at pH 9 within 48 h. Seyedi et al.[47] also identified four bacterial strains (F52, C43, C19, and C25) capable of decolorizing Disperse Blue 60 with efficiencies between 93 and 100%. These findings highlight the efficiency, sustainability, and eco-friendliness of treating industrial dye wastewater. The FTIR and GC–MS analyses confirm the breakdown of aromatic rings and azo bonds, demonstrating the potential of bacterial strains in degrading complex organic compounds. Given the significant environmental impact of textile wastewater, bioremediation offers a safer and more sustainable alternative to conventional chemical and physical methods. Further optimization of these strategies could reduce pollution and promote sustainable wastewater management.

CuNPs stabilization on bacteria strain N for AR88 dye degradation

After the fixation process, the presence of CuNPs on the surface of strain N was evaluated using SEM–EDX. The results of this analysis are presented in Fig. 9A,B, while the EDX spectrum confirms the stabilization of CuNPs on the bacterial surface (Fig. 9C). Furthermore, fixation was utilized to degrade the AR88 dye. The findings revealed that the strain containing CuNPs achieved complete (100%) degradation and removal of AR88 within 13 h. The application of metal nanoparticles, particularly CuNPs, significantly enhances the dye-removal

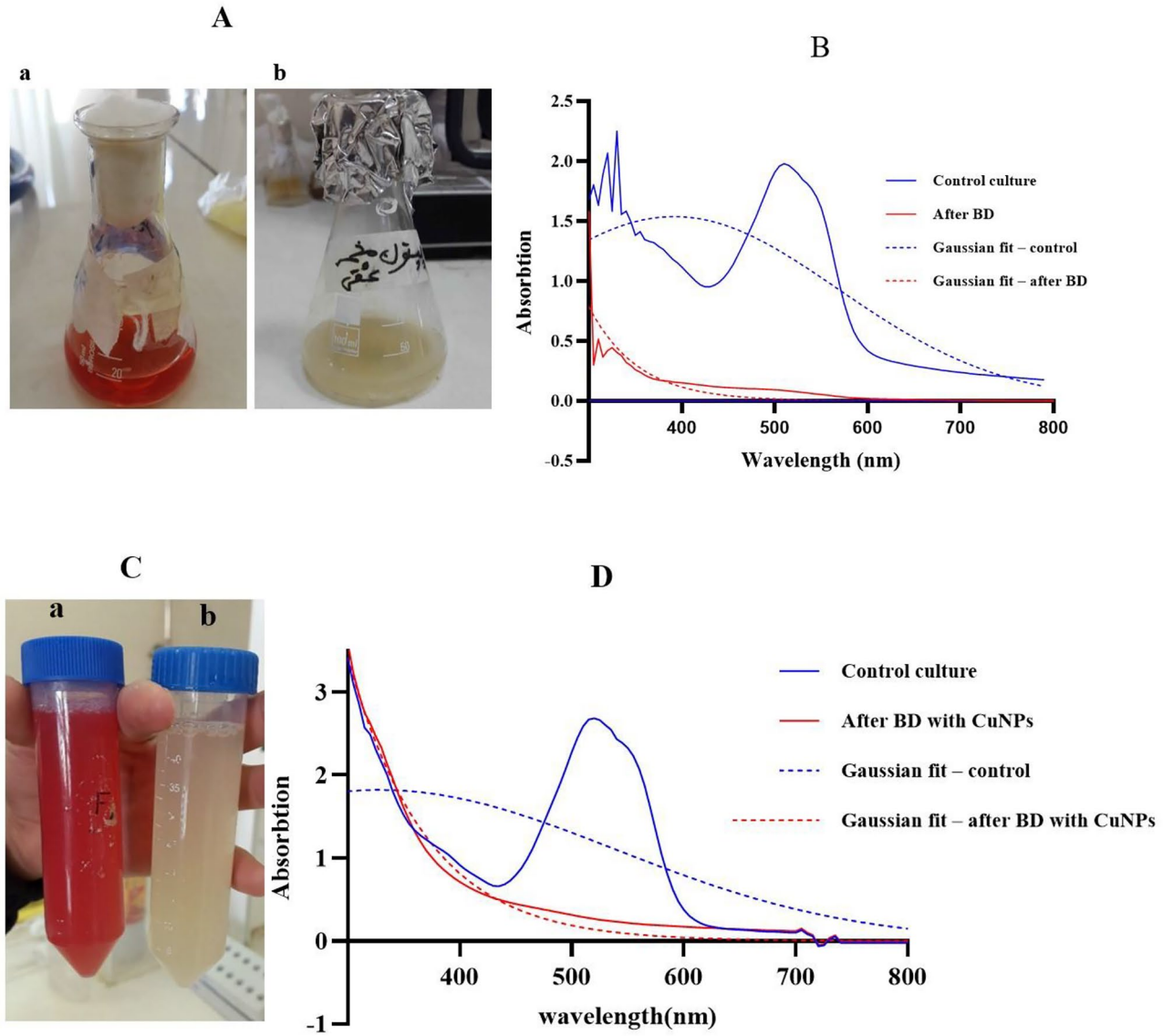

Fig. 6. (**A**) Decolorization of Acid Red 88 (AR88) without CuNPs by CFE of bacterial strain N, isolated from Kashan textile effluent: (a) control culture and (b) culture after bacterial decolorization (BD) following 24 h of incubation. **(B)** UV–Vis absorption spectra of AR88 without CuNPs before (blue) and after (red) BD by strain N after 24 h, including Gaussian fitting curves for both. (**C**) Decolorization of AR88 in the presence of CuNPs by bacterial strain N: (a) control culture and (b) culture after BD following 11 h of incubation. (**D**) UV–Vis absorption spectra of AR88 with CuNPs before (blue) and after (red) BD by strain N after 11 h, with corresponding Gaussian fit curves.

potential of bacteria. These nanoparticles act as highly efficient catalysts, accelerating the degradation process and reducing reaction times, thereby improving the biodegradation efficiency of bacteria. Moreover, stabilizing nanoparticles on the bacterial surface augments their decolorization capacity. It enhances their stability and resistance in contaminated environments, enabling them to survive and function effectively under harsh environmental conditions. These results are consistent with previous research, such as the study by Mehrzad et al.[31], which examined the stabilization of NSTO nanoparticles on strain N for the complete degradation of Blue 41 dye. Their findings similarly demonstrated that nanoparticle stabilization on bacteria resulted in rapid and complete dye degradation.

Another study showed that a bacterial consortium consisting of *Raoultella planticola*, *Ochrobactrum thiophenivorans*, *Bacillus flexus*, and *Staphylococcus xylosus* effectively degraded methyl orange under high salinity conditions. The metabolic byproducts had low toxicity, and the consortium performed well in treating agricultural and industrial wastewater[51]. Anchani et al.[19] investigated the removal of malachite green dye from water using copper oxide nanoparticles. These nanoparticles were synthesized through an environmentally friendly approach, where copper sulfate was extracted from electronic waste and reduced using banana blossom

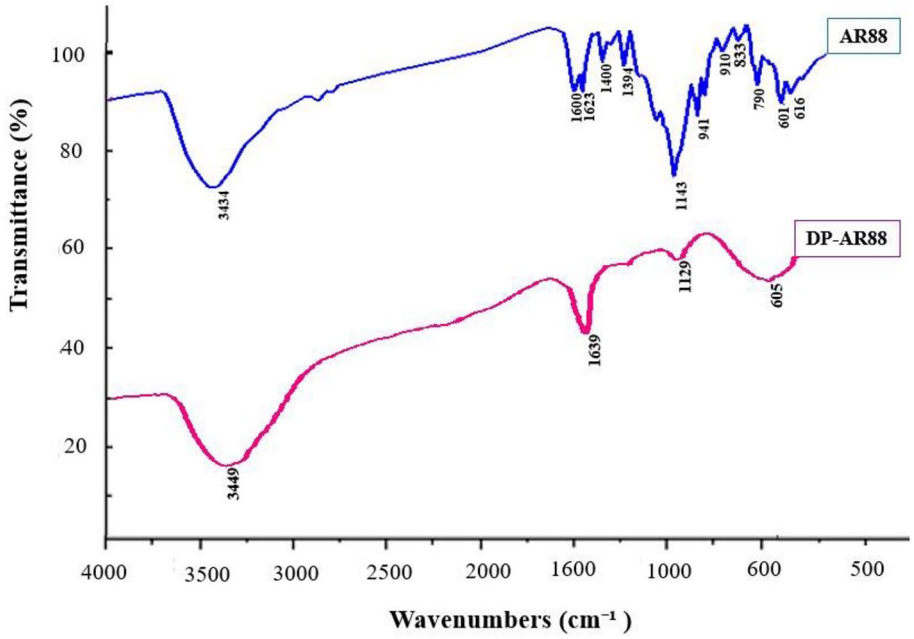

Fig. 7. The FTIR spectra of AR88 and DP-AR88.

extract. The method demonstrated a 92% efficiency in dye removal, presenting a sustainable and cost-effective solution[19].

Conclusion

This study highlights the isolation of a novel copper-tolerant strain, *Micrococcus lylae*, from the Sungun copper mine, demonstrating its potential for the biological synthesis of CuNPs. These nanoparticles exhibited potent antimicrobial activity, efficient dye degradation, and promising anti-cancer properties with minimal toxicity. Notably, combining CuNPs with *M. alkaliphilum* enhanced the degradation of the AR88 dye while reducing its toxicity. The biodegradation of AR88 was assessed under different conditions, utilizing extracellular metabolites and biomass with or without CuNPs. CuNPs were successfully anchored onto strain N, as confirmed by SEM, which revealed their presence on the outer surface of the bacterial cells. Integrating CuNPs with strain N significantly accelerated AR88 degradation, demonstrating exceptional efficiency. FTIR and GC–MS analyses confirmed the complete breakdown of AR88, while toxicity assessments using brine shrimp and seed germination assays indicated that the degradation byproducts and CuNPs exhibited low toxicity. Furthermore, CuNPs displayed strong antibacterial properties, effectively removing dyes and microbial contaminants from wastewater. These findings indicate the potential of biogenically synthesized CuNPs via *M. lylae* as a sustainable, eco-friendly solution for environmental remediation and biomedical applications.

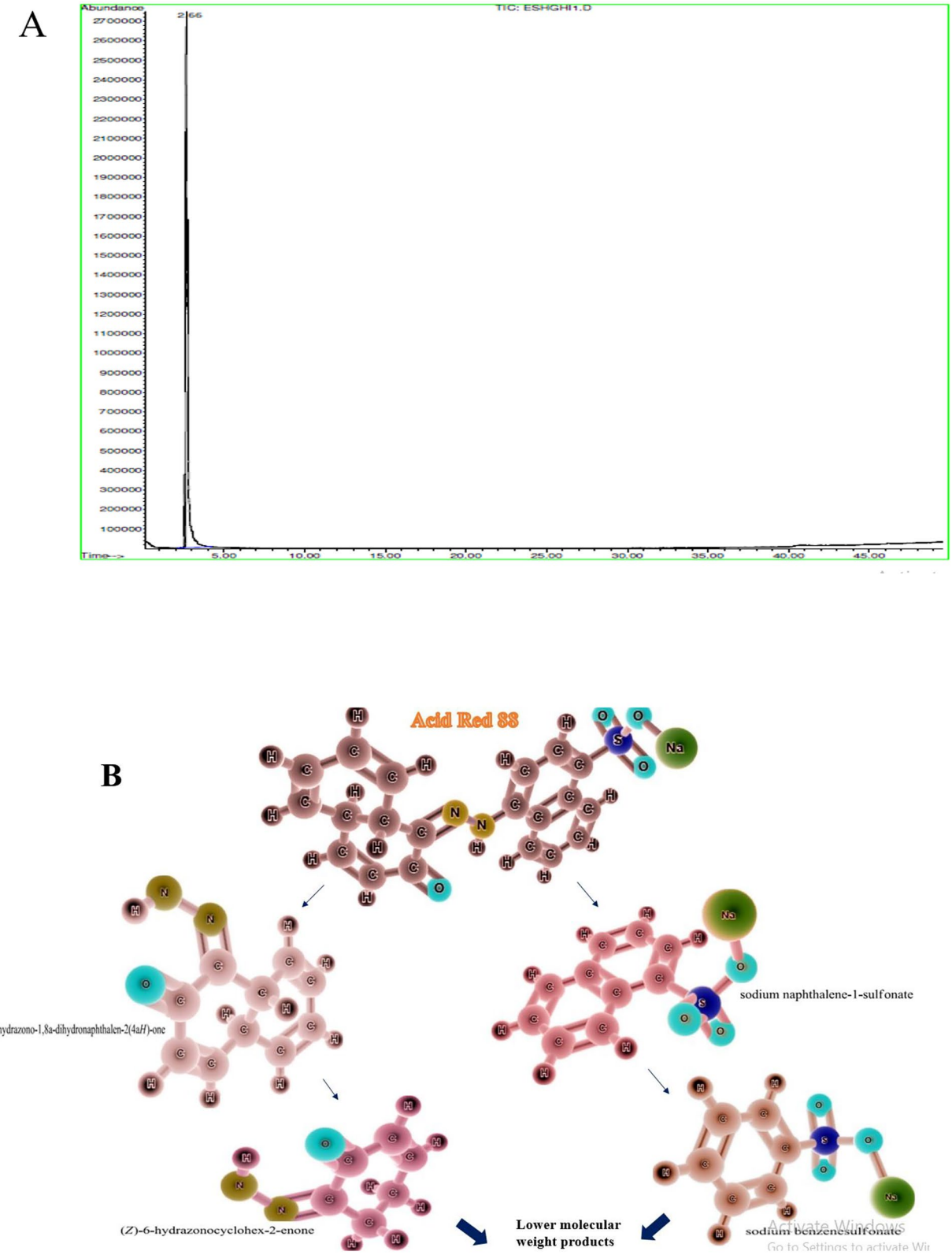

Fig. 8. GC–MS analysis of AR88 dye degradation (**A**) and AR88 dye degradation pathway (**B**).

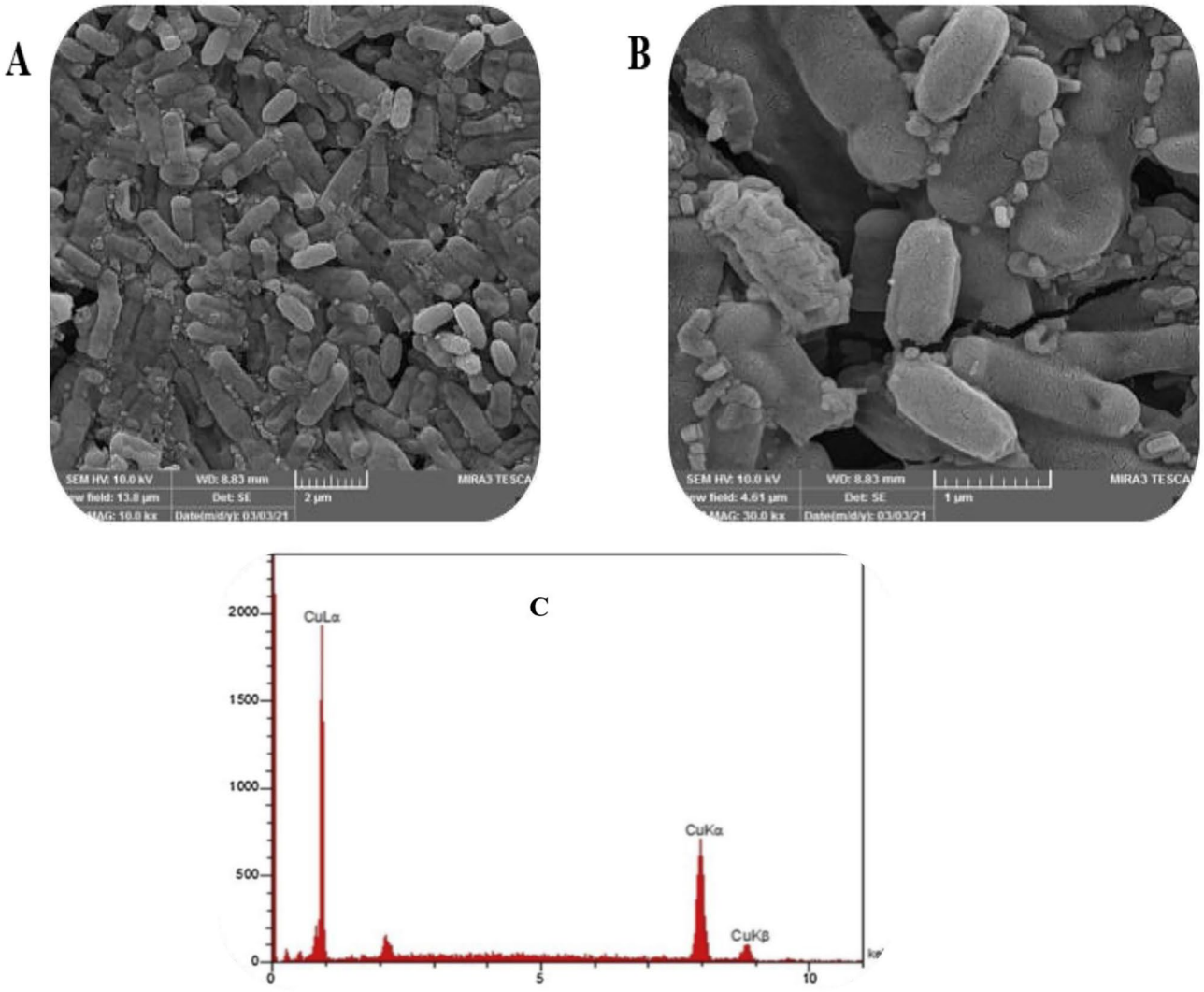

Fig. 9. SEM images of CuNPs on bacterial strain N (**A,B**), EDX spectrum that confirms the existence of CuNPs (**C**).

Data availability

The corresponding author will provide access to the datasets upon request.

Received: 18 December 2024; Accepted: 20 May 2025
Published online: 29 May 2025

References

1. Mohammad, N. M. & Salehi, R. Dye removal from colored textile wastewater using chitosan in binary systems. *Desalination* **267**, 64–72. https://doi.org/10.1016/j.desal.2010.09.007 (2011).
2. Paz, A., Carballo, J. & Perez, M. J. Domínguez, J.M. Biological treatment of model dyes and textile wastewaters. *Chemosphere* **181**, 168–177. https://doi.org/10.1016/j.chemosphere.2017.04.046 (2017).
3. Banat, I. M., Nigam, P., Singh, D. & Marchant, R. Microbial decolorization of textile-dye-containing effluents: A review. *Biores. Technol.* **58**, 217–227. https://doi.org/10.1016/S0960-8524(96)00113-7 (1996).
4. Meyer, U. Biodegradation of synthetic organic colorant. *FEMS Symp.* **12**, 371–385. https://doi.org/10.12691/ijebb-2-3-7 (1981).
5. Dellile, D., Basseres, A. & Dessomemes, A. A. Effectiveness of bioremediation for oil-pulluted Antarctic seawater. *Polar Biol.* **19**(4), 237–241. https://doi.org/10.1007/s003000050240 (1998).
6. Margesin, R. & Schinner, F. Bilogical decontamination of oil spills in cold environmination. *J. Chem. Technol. Biotechnol.* **74**(5), 381–389. https://doi.org/10.1002/(SICI)1097-4660(199905)74:5%3c381::AID-JCTB59%3e3.0.CO;2-0 (1999).
7. Ramalho, P. A., Scholze, M. H. & Cardoso, M. T. Improved condition for the aerobic reductive decolorization of azo dyes by *Candida zeylanoides*. *Enzyme Microb. Technol.* **31**(6), 848–854 (2002).
8. Supaka, N., Juntongjin, K., Damaronglerd, S., Delia, M. & Strehaiano, P. Microbial decolorization of reactive azo dyes in a sequential anaerobic–aerobic system. *J. Chem. Eng.* **99**(2), 169–176. https://doi.org/10.1016/j.cej.2003.09.010 (2004).
9. Bafana, A., Saravana Devi, S., Krishnamurthi, K. & Chakarabarti, T. Kinetics of decolourisation and biotransformation of direct Black 38 by *C. hominis* and *P. stutzeri*. *J. Microbiol. Biotechnol.* **74**(5), 1145–52. https://doi.org/10.1007/s00253-006-0751-5 (2007).

10. Asad, S., Amozegar, M. A., Pourbabaee, A. A., Sarbolouki, M. N. & Dastgheibs, M. M. Decolorization of textile azo dyes by newly isolated halophilic and halotolerant bacteria. *J. Bioresour. Technol.* **98**(11), 2082–2088. https://doi.org/10.1016/j.biortech.2006.08.020 (2007).
11. Mohana, S., Shrivastava, S. H., Divecha, J. & Madamwar, D. Response surface methodology for optimization of medium for decolorization. *J. Bioresour. Technol.* **99**(3), 562–569. https://doi.org/10.1016/j.biortech.2006.12.033 (2008).
12. Ali, N., Ikramullah, L. G. H., Hameed, A. & Ahmed, S. Decolorization of Acid Red 151 by *Aspergillus niger* S A 1 under different physicochemical condition. *J. Microbial Biotechnol.* **24**(7), 1099–1105. https://doi.org/10.1007/s11274-007-9581-6 (2008).
13. Kalyani, D. C., Telke, A. A., Dhanve, R. S. & Jadhave, J. P. Ecofriendly biodegradation and detoxification of Reactive Red 2 textile dye by newly isolated *Psedomonas* sp. SUK1. *J. Hazard. Mater.* **163**(2–3), 735–742. https://doi.org/10.1016/j.jhazmat.2008.07.020 (2009).
14. Lembre, P., Lorentz, C. & Di Martino, P. Exopolysaccharides of the biofilm matrix: A complex biophysical world. In *The Complex World of Polysaccharides, Desiree Nedra Karunaratne*. https://doi.org/10.5772/51213 (InTech, 2012).
15. Sharma, M. et al. Microbial fuel cells for azo dye degradation: A perspective review. *J. Ind. Eng. Chem.* https://doi.org/10.1016/j.jiec.2024.07.031 (2024).
16. Ma, X. et al. Copper-containing nanoparticles: Mechanism of antimicrobial effect and application in dentistry—A narrative review. *Front. Surg.* **9**, 905892. https://doi.org/10.3389/fsurg.2022.905892 (2022).
17. Khan, F. A. *Biotechnology Fundamentals* (CRC Press, 2011).
18. Heiligtag, F. J. & Niederberger, M. The fascinating world of nanoparticle research. *Mater. Today* **16**(7–8), 262–271. https://doi.org/10.1016/j.mattod.2013.07.004 (2013).
19. Anchani, A. H., Abishini, A. H. & Ashokkumar, T. A novel method for biosynthesis of copper oxide nanoparticles using banana blossom and E-waste: Characterization and application in malachite green dye removal through response surface methodology optimization. *Discov. Biotechnol.* **1**, 4. https://doi.org/10.1007/s44340-024-00004-9 (2024).
20. Dhas, N. A., Raj, C. P. & Gedanken, A. Synthesis, characterization, and properties of metallic copper nanoparticles. *Chem. Mater.* **10**(5), 1446–1452. https://doi.org/10.1021/cm9708269 (1998).
21. Ramyadevi, J., Jeyasubramanian, K., Marikani, A., Rajakumar, G. & Rahuman, A. A. Synthesis and antimicrobial activity of copper nanoparticles. *Mater. Lett.* **71**, 114–116. https://doi.org/10.1016/j.matlet.2011.12.055 (2012).
22. Wei, Y. et al. Synthesis of stable, low-dispersity copper nanoparticles and nanorods and their antifungal and catalytic properties. *J. Phys. Chem. C.* **114**(37), 15612–15616. https://doi.org/10.1021/jp1055683 (2010).
23. Din, M. I. & Rehan, R. Synthesis, characterization, and applications of copper nanoparticles. *Anal. Lett.* **50**(1), 50–56. https://doi.org/10.1080/00032719.2016.1172081 (2017).
24. Marmur, J. A procedure for the isolation of deoxyribonucleic acid from micro-organisms. *J. Mol. Biol.* **3**(2), 208–218. https://doi.org/10.1016/S0022-2836(61)80047-8 (1961).
25. Stackebrandt, E. & Goodfellow, M. *Nucleic Acid Techniques in Bacterial Systematics* (Wiley, 1991).
26. Turner, S., Pryer, K. M., Miao, V. P. W. & Palmer, J. D. Investigating deep phylogenetic relationships among cyanobacteria and plastids by small subunit rRNA sequence analysis 1. *J. Eukaryot. Microbiol.* **46**, 327–338. https://doi.org/10.1111/j.1550-7408.1999.tb04612.x (1999).
27. Eshghi, S. & Kashi, F. J. Bacterial synthesis of magnetic Fe_3O_4 nanoparticles: Decolorization Acid Red 88 using FeNPs /Ca-Alg beads. *Arab. J. Chem.* **1**, 104032. https://doi.org/10.1016/j.arabjc.2022.104032 (2022).
28. Nazari, N. & Kashi, F. J. A novel microbial synthesis of silver nanoparticles: Its bioactivity, Ag/Ca-Alg beads as an effective catalyst for decolorization Disperse Blue 183 from textile industry effluent. *Sep. Purif. Technol.* **259**, 118117. https://doi.org/10.1016/j.seppur.2020.118117 (2020).
29. Nautiyal, A. & Shukla, S. R. Silver nanoparticles catalyzed reductive decolorization of spent dye bath containing acid dye and its reuse in dyeing. *J. Water Process Eng.* **22**, 276–285. https://doi.org/10.1016/j.jwpe.2018.02.014 (2018).
30. Arulvasu, C., Jennifer, S. M., Prabhu, D. & Chandhirasekar, D. Toxicity effect of silver nanoparticles in brine shrimp Artemia. *Sci. World J.* **2014**, 919. https://doi.org/10.1155/2014/256919 (2014).
31. Mehrzad, M. et al. Novel environmental method for enhanced biodegradation of contaminated wastewater via immobilizing nanoparticles on a new bacterial strain isolated industrial textile. *J. Environ. Manag.* **1**, 116528. https://doi.org/10.1016/j.jenvman.2022.116528 (2022).
32. Dashtizadeh, Z. et al. Phytosynthesis of copper nanoparticles using *Prunus mahaleb* L. and its biological activity. *Mater. Today Commun.* **27**(6), 102456. https://doi.org/10.1016/j.mtcomm.2021.102456 (2021).
33. Khatak, S., Abhilasha, H. & Malik, D. K. Biological synthesis of copper nanoparticles using intra generic edible medicinal plants of Rosaceae family. *IJCS* **7**(3), 753–756 (2019).
34. Rakhshan, N. et al. A novel bacterial route to synthesize Cu nanoparticles and their antibacterial activity. *J. Cluster Sci.* https://doi.org/10.1007/s10876-021-02176-4(0123456789 (2021).
35. Ashrafi, M. et al. Improvement mechanical and antibacterial properties of epoxy by polyethylene glycol and Ag/CuO nanoparticles. *Polym. Compos.* **40**(9), 3393–3401. https://doi.org/10.1002/pc.25200 (2019).
36. Almahdy, A. G. et al. Methyl orange biodegradation by immobilized consortium microspheres: Experimental design approach, toxicity study and bioaugmentation potential. *Microb. Cell Fact.* **23**, 148. https://doi.org/10.1186/s12934-024-02400-6 (2024).
37. Hosseinzadeh, I. et al. Evaluation of susceptibility coefficient and death kinetics of *Escherichia coli* and *Staphylococcus aureus* to copper oxide nanoparticles. **20**, 35–85 (2012).
38. Sangeeta, M. K. et al. In-vitro evaluation of *Talaromyces islandicus* mediated zinc oxide nanoparticles for antibacterial, anti-inflammatory, bio-pesticidal and seed growth promoting activities. *Waste Biomass Valoriz.* **15**(3), 1–15. https://doi.org/10.1007/s12649-023-02386-z (2023).
39. Shashiraj, K. N. et al. Exploring the antimicrobial, anticancer, and apoptosis inducing ability of biofabricated silver nanoparticles using *Lagerstroemia speciosa* flower buds against the human osteosarcoma (MG-63) cell line via flow cytometry. *Bioengineering* **10**, 821. https://doi.org/10.3390/bioengineering10070821 (2023).
40. Kariyellappa, S. et al. Biomimetic synthesis of silver nanoparticles using *Cucumis sativus* var. hardwickii fruit extract and their characterizations, anticancer potential and apoptosis studies against Pa-1 (Human ovarian teratocarcinoma) cell line via flow cytometry. *Appl. Nanosci.* **13**, 3073–3084. https://doi.org/10.1007/s13204-022-02386-w (2023).
41. Nayaka, S. et al. Biosynthesis, characterization, and in vitro assessment on cytotoxicity of actinomycete-synthesized silver nanoparticles on *Allium cepa* root tip cells. *Beni-Suef Univ. J. Basic Appl. Sci.* **9**, 51. https://doi.org/10.1186/s43088-020-00074-8 (2020).
42. Eltarahony, M. et al. Concurrent synthesis of zero- and one-dimensional, spherical, rod-, needle-, and wire-shaped CuO nanoparticles by *Proteus mirabilis* 10B. *J. Nanomater.* **3**, 1–14. https://doi.org/10.1155/2018/1849616 (2018).
43. Eltarahony, M. et al. Unveiling the role of novel biogenic functionalized CuFe hybrid nanocomposites in boosting anticancer, antimicrobial and biosorption activities. *Sci. Rep.* **11**, 7790. https://doi.org/10.1038/s41598-021-87363-z (2021).
44. Arumugam, D. G. et al. Panchagavya mediated copper nanoparticles synthesis, characterization and evaluating cytotoxicity in brine shrimp. *Biocatal. Agric. Biotechnol.* **19**, 101132. https://doi.org/10.1016/j.bcab.2019.101132 (2019).
45. Abu-Serie, M. M. & Eltarahony, M. Novel nanoformulated diethyldithiocarbamate complexes with biosynthesized or green chemosynthesized copper oxide nanoparticles: An in vitro comparative anticancer study. *Int. J. Pharm.* **609**, 121149. https://doi.org/10.1016/j.ijpharm.2021.121149 (2021).

46. Abu-Serie, M. M. & Eltarahony, M. Novel nanoformulation of disulfiram with bacterially synthesized copper oxide nanoparticles for augmenting anticancer activity: An in vitro study. *Cancer Nanotechnol.* **12**, 25. https://doi.org/10.1186/s12645-021-00097-5 (2021).
47. Seyedi, Z. S. et al. Isolation, characterization, and decolorization of Disperse Blue 60 by newly isolated bacterial strains from Kashan textile wastewater. *Water Environ. Res.* **92**(6), 873–879. https://doi.org/10.1002/wer.1282 (2020).
48. Nazari, N. & Kashi, F. J. A novel combination of immobilized *Enterococcus casseliflavus* sp. nov. with 1 silver nanoparticles into a reusable matrix of Ca-Alg beads as a new strategy 2 for biotreatment of Disperse Blue 183: Insights into metabolic 3 characterization biotoxicity, and mutagenic properties. *J. Environ. Manag.* **325**, 116578. https://doi.org/10.1016/j.jenvman.2022.116578 (2022).
49. Nazari, N. et al. Improved application of immobilized *Enterobacter cloacae* into a bio-based polymer for Reactive Blue 19 removal, an eco-friendly advancement in potential decolorizing systems. *Water Environ. Res.* **96**(1), e10968. https://doi.org/10.1002/wer.10968 (2024).
50. Seyedi, Z. S. et al. Decolorization of Reactive Red 152 dye by native bacteria isolated from Kashan textile wastewater. *JMBS* **10**(1), 77–83 (2019).
51. Ibrahim, A. et al. Methyl orange biodegradation by immobilized ConsortiuMicrospheres: Experimental design approach, oxicity study and bioaugmentation potential. *Biology* **11**, 76. https://doi.org/10.3390/biology11010076 (2022).

Acknowledgements
We are grateful to University of Kashan for supporting this work.

Author contributions
Samira Eshghi: Research & Investigation; carried out the experiment; Data Curation; Analysis; Software and Simulation; Writing—Original Draft Preparation. Fereshteh Jookar Kashi: Idea & Conceptualization; Funding Acquisition; Methodology; Analysis; Software and Simulation; Project Administration; Supervision; Verification; Writing—Revise & Editing.

Declarations

Competing interests
The authors declare no competing interests.

Additional information
Correspondence and requests for materials should be addressed to F.J.K.

Reprints and permissions information is available at www.nature.com/reprints.

Publisher's note Springer Nature remains neutral with regard to jurisdictional claims in published maps and institutional affiliations.